Optics Letters

# High-order harmonic generations in intense MIR fields by cascade three-wave mixing in a fractal-poled $LiNbO_3$ photonic crystal

Hyunwook Park,[1,*] Antoine Camper,[1] Kyle Kafka,[1] Boqin Ma,[2,3] Yu Hang Lai,[1] Cosmin Blaga,[1] Pierre Agostini,[1] Louis F. DiMauro,[1] and Enam Chowdhury[1]

[1]Department of Physics, The Ohio State University, Columbus, Ohio 43210, USA
[2]Faculty of Science and Engineering, Communication University of China, Beijing 100024, China
[3]Laboratory of Optical Physics, Institute of Physics and Center for Condensed Matter Physics, Chinese Academy of Sciences, Beijing 100080, China
*Corresponding author: park.1771@osu.edu

Received 30 June 2017; revised 29 August 2017; accepted 1 September 2017; posted 6 September 2017 (Doc. ID 301219); published 29 September 2017

**We report on the generation of harmonic-like photon upconversion in a $LiNbO_3$-based nonlinear photonic crystal by mid-infrared (MIR) femtosecond laser pulses. We study below bandgap harmonics of various driver wavelengths, reaching up to the 11th order at 4 μm driver with 13% efficiency. We compare our results to numerical simulations based on two mechanisms: cascade three-wave mixing and non-perturbative harmonic generation, both of which include quasi-phase matching. The cascade model reproduces well the general features of the observed spectrum, including a plateau-like harmonic distribution and the observed efficiency. This has the potential for providing a source of tabletop few femtosecond ultraviolet pulses.** 

***OCIS codes:*** (190.0190) Nonlinear optics; (260.0260) Physical optics; (320.0320) Ultrafast optics; (220.0220) Optical design and fabrication.

https://doi.org/10.1364/OL.42.004020

Soon after the discovery of the laser, nonlinear light-matter interactions were demonstrated for frequency upconversion [1]. Since then, high-order nonlinear interactions have generated coherent frequency combs in gases, plasmas and, more recently, solids, extending into the soft *x*-ray range [2–5]. Despite a broad range of potential applications of a high-order harmonic light source, limitations have been imposed by poor production efficiency ($10^{-5}$ level) [6].

In general, phase matching plays the essential role in enhancing the harmonic yield [7–10]. Various phase-matching techniques have been applied to gas media, but are not always applicable to solids. Conversely, a powerful way to enhance the harmonic yield in solids is quasi-phase matching (QPM) using periodic poling in a crystal [11,12]. However, this has been effective only for high efficiency second-harmonic generation (80% conversion) [13,14] by utilizing a material with a high nonlinear susceptibility along the poling direction and a proper poling periodicity. In addition, a cascade process of sum-frequency generation (SFG) has been demonstrated to simultaneously generate second and third harmonics with relatively high efficiency [15,16]. Recently, highly efficient harmonic generations up to the eighth order of a mid-infrared (MIR) wavelength have been reported in a chirped periodically poled lithium niobate (CPPLN) crystal. Chen *et al.* interpreted their result as a series of SFG processes assisted by QPM, proposing a new approach to ultrafast broadband light sources [17].

Despite promising experimental progress, there has been a lack of detailed theoretical treatments. The absence of theoretical analysis limits fundamental understanding and, thus, restricts further applications such as optimization of the poling structure for a specific application. At this point, a fundamental question remains: is it possible to efficiently produce harmonics by non-perturbative high-order harmonic generation (NPHHG), which has been established for semiconductor crystals [5,18,19] instead of cascade SFG?

In this Letter, we report on a harmonic-*like* frequency comb generated in a fractal-poling $LiNbO_3$ (FPLN) crystal at 2, 3.6, and 4 μm driver wavelengths, verifying its generality in the ultrafast MIR regime. We have observed higher-order and larger cutoff energies than previously reported with similar efficiencies. We present two numerical simulations of wave propagation based on a cascade of second-order nonlinear processes ($\chi^{(2)}$) and NPHHG in a periodically poled domain. In comparison to the experimental results, the cascade $\chi^{(2)}$ model shows excellent agreement, in contrast to the NPHHG. From the analysis, the higher cutoff and efficiency are attributed to the existence of a higher spatial frequency of poling in our Sierpinski carpet fractal structure and a shorter crystal length, respectively, in comparison to Ref. [17]. Furthermore, we distinguished the possible cascade pathways in terms of yield,

providing a path for an optimal poling structure. Finally, we discuss possible cascade pathways for higher yield, providing another design with optimization parameters. Our understanding in designing nonlinear photonic crystals may allow the generation of a bright ultrafast vacuum ultraviolet (UV) light and open novel pathways for nonlinear light-matter coupling enhancement [20], nano-photonic waveguides [21], photon-entanglement sources [22], etc.

A fractal-structure poling is imprinted in a $LiNbO_3$ (LN) single crystal by the electric poling method [23,24], and the arrangement of the poled area is designed such that the fourth-order fractal structure is formed, as illustrated in the inset of Fig. 1. The poling direction along the $z$-axis is in the $c$-axis of the crystal and the laser polarization direction. The sample size is 8 mm × 8 mm with 0.5 mm thickness. For the 2 μm driver, we use a modified Spectra-Physics OPA-800 laser system producing 70 fs pulses centered at 2.05 μm with a power density up to 10 TW/cm$^2$. For the longer wavelength studies, a homebuilt optical-parametric amplifier system produces 100 fs pulses centered at 3.6 and 4.0 μm with a 300 nm bandwidth and a power density of 2 TW/cm$^2$. The laser beams are incident along the $x$-axis and focused by the 30 and 25 cm focal lenses. A calibrated spectrometer (Ocean Optics USB+2000) detects the harmonic emission.

Figure 1 shows the experimental geometry and the output light scattered off a white screen for a 3.6 μm driver wavelength. The emission spectral content consists of bright white light along the propagation axis and angularly dispersed visible colors diverging off-axis. The off-axis visible light can be explained by different phase-matching angles for different harmonic orders via the 2D spatial frequencies of the poling structure. This type of QPM with a 2D fractal structure has been observed in Cerenkov-type harmonic generation [25,26]. The phase matching from the red through blue colors for increasing angles is consistent with our observation, as shown in Fig. 1. Here our analysis is focused on the intense on-axis white light emission.

Figure 2 shows the on-axis white light using an intensity-calibrated spectrometer. The spectral distribution features a plateau of harmonics followed by a cutoff. The detected cutoffs are below the material bandgap of 4 eV for LN. The energy conversion efficiency is about 13%, including all harmonics, and the cutoff corresponds to the sixth, 10th, and 11th orders at

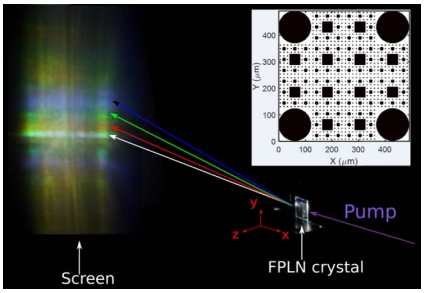


**Fig. 1.** Photograph of the experimental scheme. Inset: the fractal-poling structure of the LN crystal, where the black and white shadings represent the sign of the poling. The MIR pump propagates along the $x$-axis and is polarized in the $z$-direction. The output light is imaged on a screen placed 20 cm away.

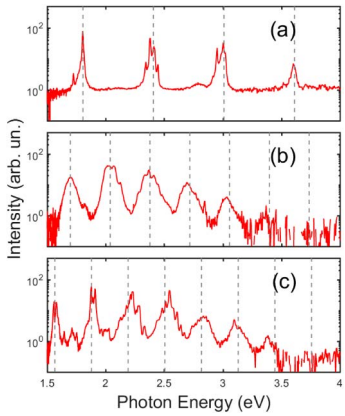


**Fig. 2.** Observed spectra along the propagation direction at (a) 2.0, (b) 3.6, and (c) 4.0 μm at room temperature. The vertical dashed lines indicate the expected harmonic energy spaced by $h\nu_C$.

2.0, 3.6, and 4 μm, respectively. In comparison to Ref. [17], the cutoff energy is higher, but with a lower efficiency.

To understand QPM in a poled crystal, it is more straightforward to describe the poling structure of the crystal in the spatial frequency domain. The crystal poling structure $f(x)$ accounting for the sign of poling as a function of position, $x$, can be written in terms of spatial frequency via a discrete Fourier transform: $f(x) = \sum_m F_m e^{iK_m x}$, where $K_m = \frac{2m\pi}{L}$ is the spatial frequency supported by a crystal with length $L$, and $F_m$ is the $m$th-order Fourier coefficient of $f(x)$. For a driver wave vector, $k$, the phase mismatch ($\Delta k$) between the driver and its $q$th harmonic order with wave vector $k_q$ can be compensated for by a spatial frequency $K_M = \frac{2\pi}{\lambda}$ with a poling period $\lambda$ so that $\Delta k = k_q - qk - K_M = 0$. If we consider a limiting case where the pump laser is not depleted during propagation and $k_q - qk = K_M$, the intensity of the $q$th harmonic field grows monotonically, and its growth rate is proportional to $F_M$. In contrast, if $k_q - qk \neq K_M$, then the intensity of the $q$th harmonic field oscillates as a function of $x$ and does not grow efficiently. Following this general principle, Chen and coworkers designed a CPPLN crystal, which forms a series of bands of various spatial frequencies, i.e., many $K_M$s. As a result, the CPPLN crystal supports phase matching for a broad driver bandwidth, producing high harmonic yields. Alternately, the existence of larger spatial frequencies (larger $K_M$ or smaller $\lambda$) helps to achieve higher orders. In our FPLN crystal, the smallest $\lambda$ period is 13.64 μm, which is shorter than the ∼28 μm used in Ref. [17], and is responsible for the higher cutoff energy.

For a more comprehensive analysis, we have developed a model based on cascade SFG and difference frequency generation (DFG) with QPM by propagating coupled wave equations, dubbed the cascade three-wave mixing (C3WM) model [11,27]. In the calculation, all field parameters are identical to the experiments and focal averaging accounts for the distribution of arrays with different poling structures within the focal volume. The C3WM numerical spectrum is obtained by propagating a fundamental field, $\mathcal{A}(0,\omega_L) = \mathcal{A}_0 e^{-\left(\frac{\omega_L-\omega_C}{\sigma}\right)^2}$, taking into account all first- and second-order processes, i.e., absorption, SFG, and DFG as follows:

$$\mathcal{A}(x+dx,\omega) = \mathcal{A}(x,\omega) - \alpha_\omega \mathcal{A}(x,\omega) + f(x)dx\frac{i\omega d_{33}}{4n(\omega)c} \times \left[\int_{\omega_0}^{\omega} d\tilde{\omega}\mathcal{A}(\tilde{\omega})\mathcal{A}(\omega-\tilde{\omega})e^{-i[k(\omega)-k(\tilde{\omega})-k(\omega-\tilde{\omega})]x'} + \int_{\omega_0}^{\omega_1-\omega} d\tilde{\omega}\mathcal{A}(\tilde{\omega})\mathcal{A}(\omega+\tilde{\omega})e^{-i[k(\omega)+k(\tilde{\omega})-k(\omega+\tilde{\omega})]x'}\right], \quad (1)$$

where $x$ is the position in the propagation direction, $d_{33}$ is the second-order susceptibility ($d_{33} = 27$ pm/V), $\alpha_\omega$ is the absorption coefficient, $n(\omega)$ is the refractive index, $c$ is the speed of light in vacuum. $\omega$ is the frequency of the generated field and $\forall\,\omega \in [2\omega_0, \omega_1 - \omega_0]$, $\omega_L$ is the laser frequency, $\sigma$ is the laser bandwidth, $\omega_C$ is the laser's central frequency, and $\omega_0$ and $\omega_1$ are the low and high limits of the frequency in the calculation, respectivy. The boundary, $[\omega_0\ \omega_1] = [0.1\ \ 4\text{eV}]$, is chosen to be below the bandgap, where the refractive index for LN is known. The second term is the absorption term, and the third and fourth terms represent the SFG and DFG processes, respectively. This model is more complete than the previous interpretation in Ref. [17], which does not consider the down-conversion process. For example, the sixth-harmonic order can be produced by DFG between the fifth to 11th orders, as well as by SFG between the fundamental and fifth orders. The blue curve in Fig. 3(a) shows the calculated spectra at 3.6 μm and well reproduces the observed spectrum (the gray curve), including the plateau-like distribution and efficiency of about 10%. Similar agreement is observed at other wavelengths. First, we find that including DFG is necessary for convergence of the calculations and good agreement with the experimental results. We find that DFG, not considered in Chen's interpretation, is physically essential. To isolate the QPM effects, the calculation is performed for a regular LN crystal. As illustrated by the red dashed curve, HHG intensity by the cascade process without QPM rapidly and monotonically decays toward the higher order, highlighting the role of QPM to reach high orders.

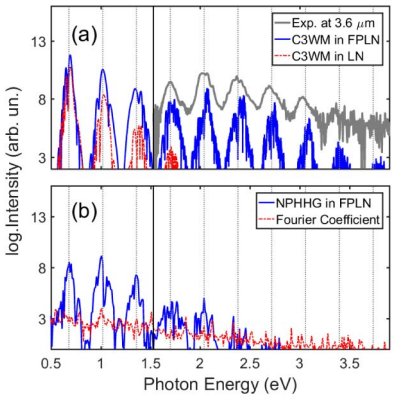


**Fig. 3.** Calculated spectra from the C3WM and NPHHG models at 3.6 μm. (a) The gray solid line is from the experiment, the blue solid line is from the C3WM model in the FPLN crystal, and the dotted red line is from a regular LN crystal. (b) The blue solid line is from an NPHHG model in the FPLN crystal, and the dotted red line is the Fourier coefficient of the FPLN. The vertical solid lines indicate the lower detection limit of our spectrometer, and the dotted lines indicate the harmonic energy.

Second, the generation of the $q$th harmonic order depends on the building up of the lower orders ($<q$) in the cascade process. As a result, the third and higher harmonics, the amplitude of the pump, cannot be considered to be constant along the direction of propagation. Consequently, we conclude that the growth rate of the harmonic field is not simply determined by the Fourier coefficients. This is clear when comparing the harmonic signal with the Fourier coefficients. For example, the second- and third-harmonics and the corresponding Fourier coefficients as a function of driver photon energy are plotted in Fig. 4(a). For the second-harmonic generation [top of Fig. 4(a)], the yield (red curve) is mainly determined by the Fourier coefficients (blue dash) for all driver energies. However, this is no longer true for the third order (and the higher orders not shown). As marked by the vertical lines in the bottom of Fig. 4(a), some peaks of the third harmonic in the yield (red curve) do not coincide with the peaks of the Fourier coefficient (blue dash). Yet, it should be noted that the growth rate of the harmonic yield is proportional to the Fourier coefficient if we limit our discussion to harmonics by $n$ identical photons ($\omega + \omega + \cdots + \omega \rightarrow n\omega$), i.e., harmonic generation from the $\chi^{(n)}$ process, with an assumption of no depletion of pump.

In comparison, we have calculated the propagation effects on NPHHG with QPM. NPHHG is driven by nonlinear oscillations of transition dipoles between valence and conduction bands, the so-called interband model [18]. Note that we do not consider NPHHG by nonlinear currents, the so-called intraband model [19], since the currents are not affected by the poling process. Here we assume that the microscopic response of the interband transition dipole is uniform through the crystal [21], and the sign of the interband polarization term is changed

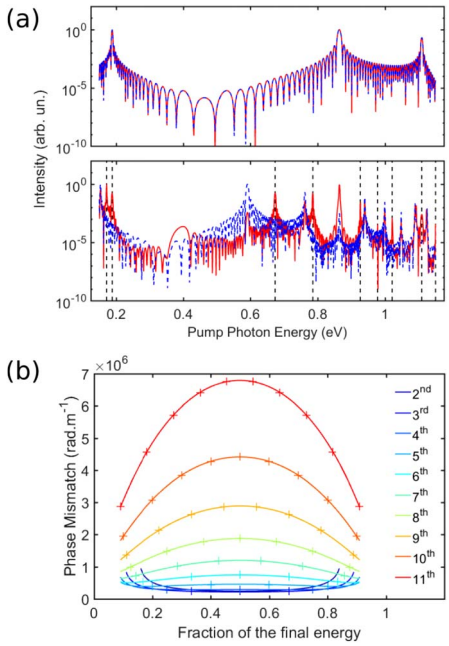


**Fig. 4.** (a) Comparison of the harmonic intensity and the Fourier coefficient as a function of driver photon energy. The red curves are the harmonic intensities (top for second harmonic and bottom for third harmonic), and the blue curves are the Fourier coefficient. (b) Phase mismatch for different harmonics at different SFG pathways. The cross points indicate examples for the 3.6 μm driver.

according to the poling. The blue curve in Fig. 3(b) shows the result. First, the intensity of the harmonics decays rapidly with the harmonic order. This is because the QPM effects in this case simply rely on the amplitude of the Fourier coefficients ($F_M$). The Fourier coefficient (red dashed curve) decreases for larger spatial frequency ($K_M$), i.e., a larger phase mismatch in higher order ($qk - k_q$). Consequently, a decrease of both the coherence length and the Fourier coefficient at the phase mismatch frequencies results in less yield enhancement by QPM in the higher-order harmonics. Therefore, we conclude that the poling frequency in our crystal is too low to provide good QPM for the NPHHG process.

Practically, the proper design of the crystal is a prerequisite, depending on the specific application. First, a higher cutoff demands a larger poling spatial frequency, i.e., a smaller poling period in order to match coherence length for a higher order. Secondly, the spatial frequency should be optimized for a specific efficient path, among others, since absorption limits the crystal length, thus restricting the number of the poling periods ($\lambda$). Figure 4(b) shows the phase mismatch as a function of photon energy in SFG for different harmonic generations. For instance, the most (the least) efficient pathway for generating the 10th order is SFG of $\omega$ and $9\omega$ ($5\omega$ and $5\omega$) to minimize the phase mismatch, while SFG of $2\omega$ and $2\omega$ ($\omega$ and $3\omega$) is the most (the least) efficient for the fourth order. The spatial frequency at $K_M = 3 \times 10^6$ rad $\cdot$ m$^{-1}$ will be a good choice to optimize the 11th order, as well as to produce 9th and 10th orders. In addition, a larger number of $\lambda$ reduces the amplitude of the Fourier coefficient, $F_m$ [16].

In conclusion, we have demonstrated high harmonic generation in a FPLN crystal, and generalized the application in the IR and MIR regimes. The primary mechanism for high-order harmonic generation with efficiencies approaching ~13% is confirmed by our C3WM model to be the cascade process with QPM. We show that the key ingredients of a poling design for an efficient broadband HHG are the existence of a small poling period and the selection of the period that minimizes phase mismatches. Engineering a new crystal based on our understanding would help to produce an intense femtosecond UV source, although characterization of the pulse needs to be performed prior to its applications.

**Funding.** National Science Foundation (NSF) (1605042); U.S. Department of Energy (DOE); Office of Science (SC); Basic Energy Sciences (BES) (DE-FG02-04ER15614, DE-SC0012462); Air Force Office of Scientific Research (AFOSR) (FA9550-16-1-0069, FA9550-15-1-0203, FA9550-16-1-0013).

## REFERENCES

1. P. A. Franken, A. E. Hill, C. W. Peters, and G. Weinreich, Phys. Rev. Lett. **7**, 118 (1961).
2. T. Popmintchev, C. Hernandez-Garcia, F. Dollar, C. Mancuso, J. A. Perez-Hernandez, J. A. M.-C. Chen, A. Hankla, X. Gao, A. L. Gaeta, M. Tarazkar, D. A. Romanov, R. J. Levis, J. A. Gaffney, M. Foord, S. B. Libby, A. Jaron-Becker, A. Becker, L. Plaja, M. M. Murnane, and H. C. Kapteyn, Science **350**, 1225 (2015).
3. F. Silva, S. M. Teichmann, S. L. Cousin, M. Hemmer, and J. Biegert, Nat. Commun. **6**, 6611 (2015).
4. J. W. G. Tisch, T. Ditmire, D. J. Fraser, N. Hay, M. B. Mason, E. Springate, J. P. Marangos, and M. H. R. Hutchinson, J. Phys. B **30**, 709 (1997).
5. S. Ghimire, A. D. DiChiara, E. Sistrunk, P. Agostini, L. F. DiMauro, and D. A. Reis, Nat. Phys. **7**, 138 (2011).
6. T. Brabec and F. Krausz, Rev. Mod. Phys. **72**, 545 (2000).
7. Ph. Balcou, P. Salieres, A. L'Huillier, and M. Lewenstein, Phys. Rev. A **55**, 3204 (1997).
8. S. Kazamias, D. Douillet, F. Weihe, C. Valentin, A. Rousse, S. Sebban, G. Grillon, F. Auge, D. Hulin, and Ph. Balcou, Phys. Rev. Lett. **90**, 193901 (2003).
9. Y. Tamaki, J. Itatani, M. Obara, and K. Midorikawa, Phys. Rev. A **62**, 063802 (2000).
10. Y. Fu, H. Xiong, H. Xu, J. Yao, Y. Yu, B. Zeng, W. Chu, X. Liu, J. Chen, Y. Cheng, and Z. Xu, Phys. Rev. A **79**, 013802 (2009).
11. J. A. Armstrong, N. Bloembergen, J. Ducuing, and P. S. Pershan, Phys. Rev. **127**, 1918 (1962).
12. D. H. Jundt, G. A. Magel, M. M. Fejer, and R. L. Byer, Appl. Phys. Lett. **59**, 2657 (1991).
13. D. Taverner, P. Britton, P. G. R. Smith, D. J. Richardson, G. W. Ross, and D. C. Hanna, Opt. Lett. **23**, 162 (1998).
14. N. G. R. Broderick, G. W. Ross, H. L. Offerhaus, D. J. Richardson, and D. C. Hanna, Phys. Rev. Lett. **84**, 4345 (2000).
15. S. Zhu, Y. Zhu, and N. Ming, Science **278**, 843 (1997).
16. B. Chen, M. Ren, R. Liu, C. Zhang, Y. Sheng, B. Ma, and Z. Li, Light Sci. Appl. **3**, e189 (2014).
17. B. Chen, C. Zhang, C. Hu, R. Liu, and Z. Li, Phys. Rev. Lett. **115**, 083902 (2015).
18. G. Vampa, T. J. Hammond, N. Thiré, B. E. Schmidt, F. Légaré, C. R. McDonald, T. Brabec, and P. B. Corkum, Nature **522**, 462 (2015).
19. S. Ghimire, A. D. DiChiara, E. Sistrunk, G. Ndabashimiye, U. B. Szafruga, A. Mohammad, P. Agostini, L. F. DiMauro, and D. A. Reis, Phys. Rev. A **85**, 043836 (2012).
20. M. Soljačić and J. D. Joannopoulos, Nat. Mater. **3**, 211 (2004).
21. B. Jalai, Nat. Photonics **4**, 506 (2010).
22. A. Yoshizawa, R. Kaji, and H. Tsuchida, Electron. Lett. **39**, 621 (2003).
23. L. E. Myers, R. C. Eckardt, M. M. Fejer, R. L. Byer, W. R. Bosenberg, and J. W. Pierce, J. Opt. Soc. Am. B **12**, 2102 (1995).
24. B. Ma, B. Chen, R. Liu, and Z. Li, J. Opt. **17**, 085503 (2015).
25. B. Ma, K. Kafka, and E. Chowdhury, Chin. Opt. Lett. **15**, 051901 (2017).
26. L. Mateos, P. Molina, J. Galisteo, C. López, L. E. Bausá, and M. O. Ramírez, Opt. Express **20**, 29940 (2012).
27. F. Hache, A. Zéboulon, G. Gallot, and G. M. Gale, Opt. Lett. **20**, 1556 (1995).